

Fast formation of anode-free Li-metal batteries by pulsed current

Katarina Cicvaric^{1,*}, Leon Merker¹, Bojing Zhang¹, Fuzhan Rahmanian¹, Miran Gaberšček², Helge Sören Stein^{1,3,*}

¹ Helmholtz Institute Ulm & Institute of Physical Chemistry, Applied Electrochemistry Group, Lise-Meitner Str. 16, 89081 Ulm Germany

² National Institute of Chemistry, Department of Materials Chemistry, Hajdrihova ulica 19, 1000 Ljubljana, Slovenia

³ present address: Technical University of Munich, School of Natural Sciences, Department of Chemistry, Lichtenbergstr. 4, Munich Data Science Institute, 85748 Garching bei München, Germany

*correspondence should be addressed to: katarina.cicvaric@kit.edu, helge.stein@tum.de

Abstract

Anode-free Li-metal batteries offer high energy density but are prone to dendrite formation during charging which can cause catastrophic failures. Ensuring dendrite-free smooth Li deposits during charging is therefore necessary. Suppressing dendrite growth can be achieved by pulsed current charging, especially during the formation cycle that largely determines the corrosion trajectory of a cell. As opposed to the constant-current technique, pulsed current techniques apply intermittently stopped current flows.

This work investigates the electroplating of metallic Li onto a Cu foil current collector under constant-current and pulsed current formation protocols. In addition to smoother, less resistive electroplated metallic Li deposits and increased Coulombic efficiency, we show that by employing an optimized pulsed current formation protocol, the formation process is accelerated by a factor of 2 compared to a C/20 protocol. Finally, by employing a simple regression coupled to experimentation, we propose the pseudo-IR-drop to be used for live adjustment of pulsed current protocols i.e., individually approach each cell at all SOC during formation.

Introduction

Lithium-ion batteries (LIBs) are dominating the markets of consumer electronics and electric vehicles ^{1, 2} however, they cannot meet requirements in terms of energy density and research is ongoing to improve battery performance and decrease costs. Anode-free lithium-metal batteries (LMBs) are considered next-generation batteries as they promise high energy density. In the anode-free configuration, Li⁺ ions are extracted from a cathode and electroplated as metallic Li onto a bare Cu foil current collector during charging, resulting in a Li-metal battery configuration, while during discharging, metallic Li is stripped from the Cu foil and intercalated back into the cathode. The absence of Li-ion intercalation anode material enables thinner cells with lower weight, thus increasing both volumetric and gravimetric energy density, and reducing cost ^{3, 4, 5}. In addition, Li metal has the highest known theoretical specific capacity, low density and lowest absolute electrode potential ⁶. However, during electroplating, Li metal tends to form irregular structures as Li nucleation occurs preferentially at energetically convenient sites. As electroplating proceeds, the nuclei continue to grow and

their electric field increases attracting more Li ions from the electrolyte, forming a rough and porous Li film. This process is more pronounced by increasing electroplating current density. The excessive growth of irregular Li structures can lead to growth of Li whiskers dubbed “dendrites”^{7, 8, 9}. The rough and irregular metallic Li film has a high surface area in contact with the liquid organic electrolyte. Since Li metal can react with the organic solvents present in the electrolyte forming a well-known solid-electrolyte interface (SEI), the reaction leads to active Li loss which ultimately decreases the Coulombic efficiency. Furthermore, the needle-like dendrites can fall off the metallic Li film resulting in so-called “dead lithium” leading to further capacity loss. Even worse, extreme dendrite growth can pierce through the separator leading to a short-circuit of the cell and possibly a fire^{10 11}. Drvarič Talian et al.¹² employed a transition line model describing the impedance response of metallic Li in contact with the electrolyte to study the dynamics of surface processes upon cycling. In this work, dendrites are divided into “live porous lithium” containing active lithium covered with SEI on the surface, and “dead porous lithium” at the electrolyte side containing passivated lithium consisting of SEI-like components electronically and ionically disconnected from the bulk active lithium. It is shown that as the thickness of dead lithium increases and the electrolyte dries out, the overall resistance of a cell increases significantly, which is a consequence of extensive lithium passivation.

To improve the performance of anode-free Li-metal batteries, several strategies have been suggested in the literature, such as: modification of the current collector, creation of artificial SEI, optimization of electrolyte formulations and modification of the cycling protocol^{3, 4}. Some of the work on current collector modification strategy include investigation of other metals¹³ and alloys¹⁴, or applying coatings such as lithophilic Ag nanoparticles¹⁵ and SiOx¹⁶ oxide layer which can improve Li wettability favouring more compact and uniform metallic Li deposits. Another approach is incorporating Si₃N₄ nanoporous medium¹⁷ or modifying Cu foil with C shells with Au nanoparticles¹³ to suppress dendrite growth. Several reports propose 3D structured microporous Cu current collectors for promoting homogeneity of current distribution and hence prevent Li dendrite growth¹⁸. Artificial SEI formation strategy is realized by applying protective coating onto the Cu surface, such as polyethylene oxide¹⁹, multilayer graphene²⁰, and graphene oxide²¹ which accommodate Li deposits and reduce Li surface passivation, or Al₂O₃ layer²² which improves electrochemical stability of liquid electrolytes. Performance improvements were also attempted by modification of conventional carbonate-based electrolyte with 1 M LiPF₆, for instance, with dual salt LiDFOB/LiBF₄ liquid electrolyte²³, dual additives KPF₆/Tris (trimethylsilyl) phosphite²⁴ and dual salt LiFSI/LiTFSI ether solution²⁵. Modification of the cycling protocol strategy considers changing parameters such as cut-off voltages²⁶ or employing pulsed current instead of constant-current charging.

Herein, we propose not to alter the chemistry but solely the electrochemical procedure to assess whether or not a first-order improvement can also be achieved. Pulsed current charging protocols can improve performance of anode-free Li-metal battery as it produces smoother and more compact electroplated films compared to constant current protocols. This has been demonstrated not only in LMBs cycling^{27, 28, 29, 30} but also in the formation of SEI on graphite^{31,32}, and electroplating of various metals^{33, 34, 35} and semiconductors³⁶. During electroplating with constant current, the metal ions at the electrode surface are constantly consumed and their concentration decreases. As the plating proceeds, the constant consumption of metal ions leads to a depletion of ions at the electrode surface. The higher the current density, the higher the rate of consumption of metal ions. The adsorbed metal ions are energetically

unstable and tend to move towards already formed clusters, increasing the surface irregularities. In contrast to the constant-current protocol, the pulsed current consists of alternating constant current for a certain period of on-time, and off-time, during which the current density is 0. During the off-time, the concentration of metal ions at the electrode surface is being replenished, reducing the depletion layer. When the current is switched on again, the higher concentration of metal ions at the electrode surface hinders the mobility of the metal ions along the surface. Consequently, the deposits exhibit finer grains and a smoother surface as a result of reduced mobility of adsorbed ions at the electrode surface^{37, 38}.

Battery formation is an initial charge and discharge process in which a solid-electrolyte interface (SEI) layer is formed, typically on an anode. Conventionally, the formation is carried out for several charge and discharge cycles at very low currents of C/20 to C/10 taking days to complete³⁹. In this work, we investigate the effects of constant current and pulsed current formation on the morphology and impedance of electroplated metallic Li on Cu foil current collectors in anode-free lithium-metal coin cells, as well as the Coulombic efficiency after formation. We show the difference in morphology of metallic Li electroplated at constant-current compared to that obtained with pulsed current charging, with smoother pulse-plated films exhibiting a lower resistance and a higher Coulombic efficiency. Furthermore, the time required to complete the formation cycle is more than halved by employing an optimised pulsed current formation protocol compared to the conventional constant-current C/20 protocol. The protocol is compatible with LIBs manufacturing, carried out without modifying the conventional chemistry, nor modifying Cu current collector with additional material which adds weight and volume or additional processing step of the Cu foil. In addition, by using a regression model, we propose the *pseudo*-IR-drop parameter as a potential control feature to further improve the Coulombic efficiency and reproducibility through a customized pulsed formation protocol.

Results and discussion

Surface morphology of electroplated metallic Li

To investigate morphology of metallic Li electroplated on a Cu foil current collector, constant-current (Fig 1. a) at C/20 and C/5, and pulsed current (Fig 1. b) at C/8 with on-time 1 s and off-time 2 s, and C/5 and C/2 both with on-time 0.25 s and off-time 0.75 s charging protocols were carried out.

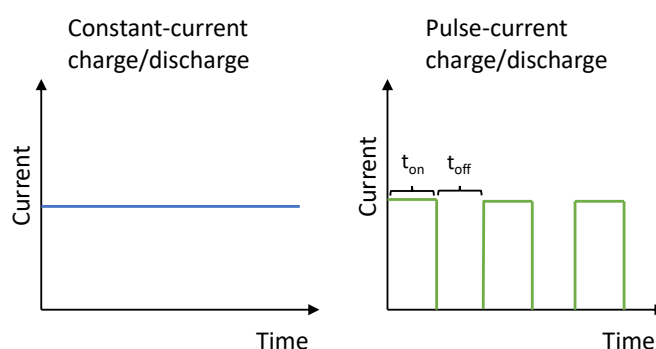


Figure 1. Schematic representation of a) constant current, and b) pulsed current electroplating.

Figure 2 shows scanning electron microscopy (SEM) micrographs of metallic Li electroplated at constant currents, C/20 (Fig 2. a, c) and C/5 (Fig 2. b, d).

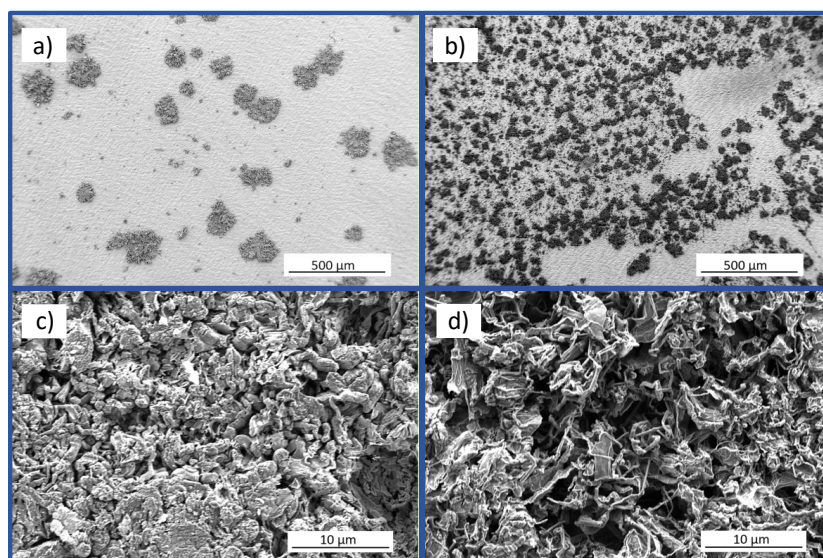


Figure 2. SEM micrographs showing morphology of metallic Li after constant-current charging onto Cu foil current collector in anode-free Li-metal coin cell in 1 M LiPF₆ in ethylene carbonate:ethyl methyl carbonate (30:70 wt%) with 2 wt% vinyl carbonate electrolyte solution at C/20 (a, c) and C/5 (b, d). The magnification of micrographs is 100 times (a, b) and 5000 times (c, d).

As can be seen in the figures (Fig. 2. a, b and Fig. 3. a, b, c), metallic Li is electroplated as separate islands rather than continuous films, probably due to low Li content (charge capacity approx. 0.2 mAh/cm²). It can also be seen that the higher substrate coverage with smaller islands is achieved at high C/5 current (Fig. 2. b) compared to low C/20 current (Fig. 2. a). Furthermore, the morphology of the islands grown at low C/20 current (Fig. 2. c) is smoother and the grains are more compact than at high C/5 current (Fig. 2. d) with sharp, “needle-like” grains. Figure 3 shows SEM micrographs of metallic Li electroplated at pulsed current C/8 with on-time of 1 s and off-time of 2 s (Fig. 3. a, d), C/5 with on-time of 0.25 s and off-time of 0.75 s (Fig. 3. b, e), and C/2 with on-time of 0.25 s and off-time of 0.75 s (Fig. 3. c, f).

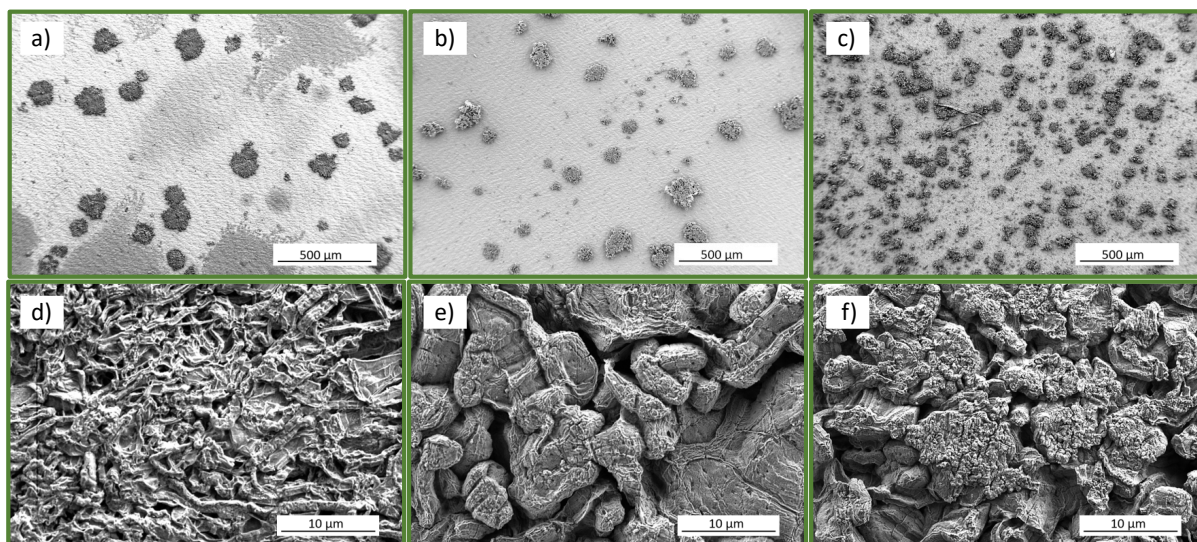


Figure 3. SEM micrographs showing morphology of metallic Li after pulsed current charging onto Cu foil current collector in anode-free Li-metal coin cell in 1 M LiPF₆ in ethylene carbonate:ethyl methyl carbonate (30:70 wt%) with 2 wt% vinyl carbonate electrolyte solution at C/8 with $t_{on}=1$ s, $t_{off}=2$ s (a, d), C/5 with $t_{on}=0.25$ s, $t_{off}=0.75$ s (b, e) and C/2 with $t_{on}=0.25$ s, $t_{off}=0.75$ s (c, f). The magnification of micrographs is 100 times (a, b, c) and 5000 times (d, e, f).

We observe an improvement of surface coverage by applying a higher current, with the highest current C/2 (Fig. 3. c) producing the smallest and densest islands compared to C/5 and C/8 (Figs. 3. b and a, respectively). This behaviour is in accordance with theory, as the nucleation rate is increased at higher current densities compared to lower current densities³⁸. Comparing the morphology of the islands, C/5 and C/2 pulse-currents with millisecond pulses produce more compact, smoother, and larger “rock-like” grains (Fig. 3. e and f, respectively), while C/8 with seconds-long pulses produce sharp, needle-like grains (Fig. 3. d). Furthermore, comparing the morphology of pulsed C/5 and C/2 islands (Fig 3. e and f) with conventional constant-current C/20 charging (Fig. 2. c), larger, smoother, and more compact grains are obtained with the pulsed charging protocol. The estimated number of Li monolayers per 0.25 s on-time is 0.16 and 0.05 for C/2 with $t_{on}=0.25$ s, $t_{off}=0.75$ s and C/5 with $t_{on}=0.25$ s, $t_{off}=0.75$ s protocols, respectively. The increase in deposited Li by approx. factor of 3 is expected as the current density applied in the C/2 protocol is approx. 3 times higher than in the C/5 protocol. For C/8 with $t_{on}=1$ s, $t_{off}=2$ s protocol the estimated number of monolayers per 1 s on-time is 0.08, which is close to the estimated value for C/5 with $t_{on}=0.25$ s, $t_{off}=0.75$ s. However, the longer off-time of 2 s could allow for surface diffusion and rearrangements of deposited Li leading to rough, “needle-like” morphology (Fig. 3 d), which differs significantly from “rock-like” grains obtained by C/5 with $t_{on}=0.25$ s, $t_{off}=0.75$ s (Fig. 3 e).

Electrochemical impedance spectra of electroplated metallic Li

Figure 4. shows electrochemical impedance spectra taken after Li electroplating onto Cu foil current collector (Fig 4. a) and the corresponding simplified equivalent electrochemical circuit (Fig 4. b). The latter was constructed based on a physical transmission line model for porous electrodes, in particular porous lithium electrode after cycling (reference 12). The meaning of

the simplified elements is as follows: R_1 represents the parallel resistance created by the movement of active ion (lithium ion) and counter charge in the separator under the external electric field. In the case of formation of the so-called dead lithium (porous inactive passive structures), R_1 also contains a contribution of migration of active and non-active charges in such “dead” porous system (reference 12). R_2 can be approximated by (reference 12):

$$R_2 = \sqrt{R_{\text{par}}R_{\text{SEI}}} \coth \sqrt{R_{\text{par}}/R_{\text{SEI}}} \quad (1)$$

where

$$R_{\text{par}} = \frac{R_{\text{live1}}R_{\text{live2}}}{R_{\text{live1}}+R_{\text{live2}}} \quad (2)$$

with R_{live1} and R_{live2} representing the transport of active (Li ion) and non-active ions, respectively, inside the pores of live Li dendrites (i.e. dendrites that still contain electronically connected metallic lithium). R_{SEI} denotes the transport resistance through the thin SEI film covering the live dendrites¹². CPE1 can be considered as an approximation of the capacitive properties of the interface between electrolyte and live dendrites. The physical meaning of R_3 can be roughly described with the following equation:

$$R_3 = \sqrt{R_{\text{live1}}R_{\text{SEI}}} \coth \sqrt{R_{\text{live1}}/R_{\text{SEI}}} \quad (3)$$

CPE2 roughly corresponds to the chemical capacitance due to chemical diffusion of species in the pores of live dendrites. Finally, element CPE3 roughly replaces at least two further low-frequency diffusional phenomena, i.e. the chemical diffusion of mobile species in dead lithium (if present) and the chemical diffusion in porous separator (see reference 12).

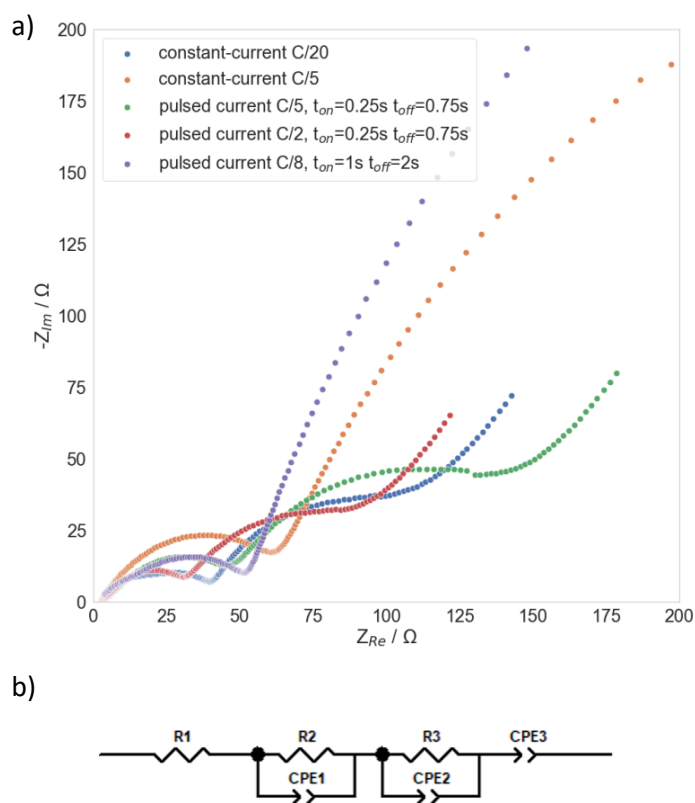


Figure 4. Electrochemical impedance spectra of metallic Li electroplated onto Cu foil current collector in anode-free Li-metal coin cell in 1 M LiPF_6 in ethylene carbonate:ethyl methyl

carbonate (30:70 wt) with 2 wt% vinyl carbonate electrolyte solution at different constant-current and pulsed current charging protocols (a) and an approximate equivalent electrochemical circuit derived from a general physics-based transmission line for porous lithium structures (see Ref. 12) (b).

Table 1. shows the resistance values of electroplated metallic Li obtained at different constant-current and pulsed current protocols. The values of resistances were obtained by fitting the experimental data to the proposed simplified equivalent circuit (Fig 4. b). The lowest resistances are obtained by employing pulsed current C/2 with on-time of 0.25 s and off-time of 0.75 s, while the highest values are for Li electroplated with pulsed current C/8 with on-time of 1 s and off-time of 2 s. Moreover, Table 1 shows the average Coulombic efficiencies and sample standard deviations of three cells after the formation cycle, where both charging and discharging were carried out with the same constant-current or pulsed protocol. As can be seen from the table, the Coulombic efficiency decreases with increasing resistance, which is most evident for the constant-current C/5 and pulsed current C/8 $t_{on}=1$ s, $t_{off}=2$ s protocol. This is probably due to the increased roughness of electroplated Li, as can be seen from the SEM images (Fig 2. d and Fig 3. d). Consequently, rougher Li deposits have a larger surface area exposed to the solvent and form a passivated Li (SEI layer), resulting in increased resistance and higher active Li loss. In addition, the highly resistive, rough deposits obtained by pulsed current C/8 with on-time of 1 s and off-time of 2 s and with constant-current C/5 electroplating exhibit poor reproducibility, as indicated by the high standard deviation in Table 1. It should also be noted that the lot of cells formed under these conditions failed due to dendrite growth and the resulting short circuit. Conversely, the smoother deposits with lower resistance obtained by constant-current C/20, pulsed current C/5 and C/2 both with on-time of 0.25 s and off-time 0.75 s (Fig 2. c, Fig 3. e and f, respectively) exhibit significantly higher Coulombic efficiency and improved reproducibility. Importantly, using C/2 with on-time of 0.25 s and off-time of 0.75 s not only the Coulombic efficiency increased by approx. 10%, but also more than halved the time needed to carry out the formation compared to the conventionally used constant-current C/20 protocol.

Table 1. Resistances obtained from fitting to equivalent electrochemical circuit and corresponding Coulombic efficiencies after formation process for various constant-current and pulsed current protocols.

Formation protocol	R_2 / Ω	R_3 / Ω	Average Coulombic efficiency± sample standard deviation
Constant-current C/20	38.8	54.4	0.73±0.04
Constant-current C/5	55.2	321.4	0.65±0.08
Pulsed current C/8 $t_{on}=1$ s, $t_{off}=2$ s	45.7	624.8	0.53±0.14
Pulsed current C/5 $t_{on}=0.25$ s, $t_{off}=0.75$ s	45.2	83.1	0.73±0.04
Pulsed current C/2 $t_{on}=0.25$ s, $t_{off}=0.75$ s	28.7	52.7	0.83±0.04

Regression and descriptor

To find an appropriate combination of input parameters to further boost the Coulombic efficiency after formation, XGBoost regression was used, considering the charge and discharge rate and the on- and off-time as input features and the Coulombic efficiency as output parameter. For this purpose, 47 coin cells were formed by pulsed charging and discharging at charging rates ranging from 1C to C/8, discharging rates ranging from 1C to C/16, on-times ranging from 0.25 s to 4 s, and off-time ranging from 0.75 s to 8 s with test-train split 80-20. Figure 5. shows prediction results of the model yielding a low R^2 score of 0.45.

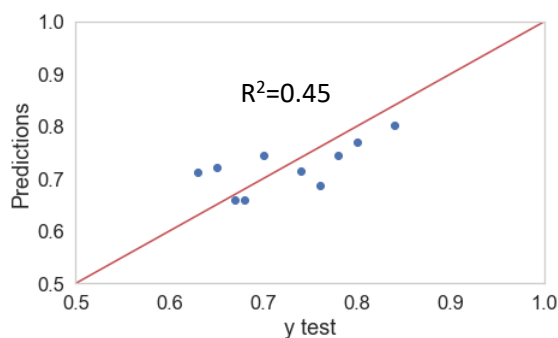


Figure 5. XGBoost regression predictions of Coulombic efficiency trained on pulsed current formation protocols in anode-free Li-metal coin cell in 1 M LiPF₆ in ethylene carbonate:ethyl methyl carbonate (30:70 wt) with 2 wt% vinyl carbonate electrolyte solution with charge rate, discharge rate, on-time and off-time as input features.

The low R^2 score of 0.45 (<0.5) means that the fit is weak and that the model should not be used for predictions. The reason for this result is poor reproducibility of the output parameter if charge and discharge rate and on-time and off-time are used as input features. Namely, it has been observed experimentally that different pulsed protocols often produce the same or very similar Coulombic efficiencies, although on average certain pulsed protocols produce an improvement. In an attempt to find input parameters that could better explain the process and could therefore be used to predict Coulombic efficiency, the voltage curve was taken into consideration. More specifically, the voltage value at the end of current on-time and voltage value at the end of current off-time that encompasses the IR-drop and off-time, which we refer to as the *pseudo-voltage*(IR)-drop (Fig. 6. a). The reason for choosing these particular points is to find a suitable off-time so not to keep the charging for too long to further reduce the time necessary for formation, but to keep it long enough for the replenishment of metal ions to occur to in order to boost Coulombic efficiency. Multiple values of *pseudo*-IR-drop were taken as input parameters along charge and discharge curves, mainly at the points on the curves where the values change the most.

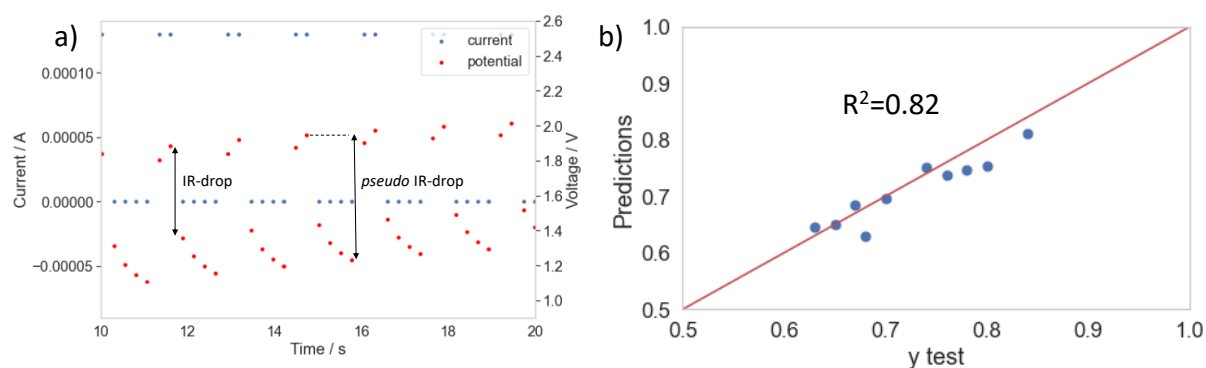


Figure 6. *Pseudo-IR-drop* representation on experimental pulsed current and voltage data (a), XGBoost regression predictions of Coulombic efficiency trained on pulsed current formation protocols in anode-free Li-metal coin cell in 1 M LiPF₆ in ethylene carbonate:ethyl methyl carbonate (30:70 wt) with 2 wt% vinyl carbonate electrolyte solution with *pseudo-IR-drop* as input feature (b).

In this case, the XGBoost regression model resulted in R^2 value of 0.82 (Fig 6. b), indicating that the fit is strong ($R^2 > 0.7$) and that the model predicts the dependent variable well, demonstrating the potential applicability of *pseudo-IR-drop* as a control parameter to achieve the desired Coulombic efficiency. It is likely that the high IR-drop corresponds to the formation of a rough metallic Li surface, since rough films possess higher resistances than smooth films, and could potentially be used to apply a reverse pulse to discharge dendrites. In this way, we hope that the *pseudo-IR-drop* could serve as a feedback loop to adjust the pulse magnitude/duration during charging to enable better control over Li electroplating and obtain smooth films. In this way, each cell could be treated individually with an appropriate procedure to boost capacity retention and reproducibility.

Conclusion

Metallic Li was electroplated onto a Cu foil current collector in an anode-free Li-metal coin cell by constant-current and pulsed current formation protocols. It is shown that smoother deposits can be obtained by using an optimised pulsed current protocol compared to constant-current protocols. After the complete formation cycle the obtained Coulombic efficiency of the optimised pulsed current formation C/2 with on-time of 0.25 s and off-time of 0.75 s protocol is approx. 10% higher than that of the conventional C/20 constant-current formation protocol. This is likely due to the obtained smoother metallic Li deposits with lower surface area and therefore less active Li loss due to the passivation reaction with the solvent. Moreover, the time necessary to complete the formation process is more than halved compared to the conventional, C/20 constant-current formation protocol. Furthermore, we show that reproducibility between the cells is poor, although on average the pulsed current formation protocol improves the Coulombic efficiency. This is confirmed using XGBoost regression, which shows very weak agreement between predictions and test values if charge and discharge rate, and on and off-times are used as input features. A strong agreement between predictions and test values was achieved if *pseudo-IR-drop* was used as an input feature. Hence, the Coulombic efficiency of the formation process could be explained and potentially predicted from *pseudo-IR-drop* by XGBoost regression. Namely, the high IR-drop

during pulsed charging is likely due to the formation of rough deposits and consequently the large surface area of the passivated Li, which has higher resistance than smooth Li deposits. In addition, we joined IR-drop with off-time into *pseudo*-IR-drop in order to find an optimal off-time for metal ion replenishment. In this way, the pulsed current protocol could potentially be tailored to each cell individually, with appropriate off-time and/or reverse pulse to discharge the dendrites.

Materials and methods

Electrode preparation

Carbon-coated LiFePO₄ (LFP) powder, Super P conductive carbon black, and carboxymethyl cellulose were purchased from a commercial supplier AOT Battery, China. The materials were used for the preparation of cathode slurry as delivered. The cathode slurry was prepared by mixing LiFePO₄ powder, Super P conductive carbon black and 2 wt% carboxymethyl cellulose aqueous solution in wt% 85, 10 and 5, respectively. The slurry was mixed in centrifugal mixer (Thinky Mixer ARE-250, USA) at 2000 rpm for 10 minutes followed by defoaming at 400 rpm for 1 minute. The mixing procedure was then repeated again. Screen printing of the cathode slurry was carried out on 16 μm thick Al foil (AOT Battery, China) by doctor blade. The thickness of the coating was set to 50 μm and applied at 60 °C with a coating speed of 5 mm/s. The coatings were then dried overnight in an oven at 140 °C. Calendering of the coatings was carried out at 30 °C (MTI MSKH-RP-1A, China). The coatings were cut into 14 mm diameter disc using a disc puncher (AOT Battery, China) to serve as cathodes in coin cells. The cathodes were weighed prior to assembly to calculate specific capacity. A 9 μm thick copper foil (AOT Battery China) was cut with the disc puncher into 15 mm diameter discs that served as anodes. Polyester/Al-oxide sheet (Freudenberg Performance Materials) was cut into a 16 mm diameter disc that served as the separator. The prepared electrodes and separator were dried overnight 80 °C in an oven.

Coin cell assembly

The LFP|Cu electrodes were assembled into CR2032 coin-type cells in a nitrogen-filled glovebox (GS Glovebox Systemtechnik, Germany). To facilitate the reproducibility and productivity of cell assembly, an in-house developed robotic cell assembly system AutoBASS was employed for the massive cell manufacturing. Detailed AutoBASS coin cell assembly procedure is described in Zhang *et al.*⁴⁰. Prior to assembly the coin cell parts (Pi-KEM, UK) were washed in an ultrasonic bath filled with isopropanol and left to dried in an oven at 80°C overnight. Pick and stack of the cell components were accomplished by a 6-axis robotic arm (Mecademic, Canada) with a linear motor axis (Jenny Science, Switzerland). Dispersing of electrolyte was completed by a second robot with an automatic liquid handling dispenser (Sartorius AG, Germany). Automatic sealing of the cells was done by the digital electric crimper (MTI, USA) modified with a microcontroller. As an electrolyte 35 μl of 1 M LiPF₆ in ethylene carbonate:ethyl methyl carbonate (30:70 wt%) with 2 wt% vinyl carbonate electrolyte (E-lyte, Germany) was added per coin cell. The cells were stored with anode side facing down for wetting for at least 24 h prior to electrochemical experiments.

Electrochemical experiments

Charge and discharge experiments were carried on LFP|Cu coin cell out using an Arbin battery tester under atmospheric conditions. Electrochemical impedance spectroscopy measurements were carried out after the first charge cycle using the PalmSens4 potentiostat/galvanostat in the frequency range of 1 MHz to 0.1 Hz with an amplitude voltage of 10 mV.

Morphology analysis

Prior to morphology analysis, coin cells were disassembled with a crimper (MTI MSK-160E, China) inside a glovebox and the anode was rinsed with EMC. The Li anode was transferred into scanning electron microscope (Thermo Fisher Scientific, USA) for surface morphology examination. The scanning electron microscopy images were taken at 2 kV acceleration voltage.

Data Availability Statement

The raw data and analysis scripts are available at <https://zenodo.org/record/8276087> under the DOI of 10.5281/zenodo.8276087 as well as the analysis code used to generate the figures.

Acknowledgements

KC, LM, BZ received funding from the European Union's Horizon 2020 research and innovation programme under grant agreement No 957189. The project is part of BATTERY 2030+, the large-scale European research initiative for inventing sustainable batteries for the future. The authors acknowledge BATTERY 2030+ funded by European Union's Horizon 2020 research and innovation program under Grant Agreement No. 957213.

References

- 1 G. Zubi, R. Dufo-López, M. Carvalho and G. Pasaoglu, *Renewable and Sustainable Energy Reviews*, 2018, **89**, 292–308.
- 2 A. Manthiram, *ACS Cent Sci*, 2017, **3**, 1063–1069.
- 3 C. Heubner, S. Maletti, H. Auer, J. Hüttel, K. Voigt, O. Lohrberg, K. Nikolowski, M. Partsch and A. Michaelis, *Adv Funct Mater*, 2021, 31.
- 4 R. V. Salvatierra, W. Chen and J. M. Tour, *Advanced Energy and Sustainability Research*, 2021, **2**, 2000110.
- 5 J. Qian, B. D. Adams, J. Zheng, W. Xu, W. A. Henderson, J. Wang, M. E. Bowden, S. Xu, J. Hu and J. G. Zhang, *Adv Funct Mater*, 2016, **26**, 7094–7102.
- 6 L. A. Selis and J. M. Seminario, *RSC Adv*, 2019, **9**, 27835–27848.
- 7 S. Li, Z. Luo, L. Li, J. Hu, G. Zou, H. Hou and X. Ji, *Energy Storage Mater*, 2020, **32**, 306–319.
- 8 T. Fuchs, J. Becker, C. G. Haslam, C. Lerch, J. Sakamoto, F. H. Richter and J. Janek, *Adv Energy Mater*, 2023, **13**, 2203174.

- 9 B. Thirumalraj, T. T. Hagos, C. J. Huang, M. A. Teshager, J. H. Cheng, W. N. Su and B. J. Hwang, *J Am Chem Soc*, 2019, **141**, 18612–18623.
- 10 Z. Xie, Z. Wu, X. An, X. Yue, J. Wang, A. Abudula and G. Guan, *Energy Storage Mater*, 2020, **32**, 386–401.
- 11 K. Liu, Y. Liu, D. Lin, A. Pei and Y. Cui, *Sci. Adv.*, 2018, **4**:eaas982.
- 12 S. Drvarič Talian, J. Bobnar, A. R. Sinigoj, I. Humar and M. Gaberšček, *Journal of Physical Chemistry C*, 2019, **123**, 27997–28007.
- 13 K. Yan, Z. Lu, H. W. Lee, F. Xiong, P. C. Hsu, Y. Li, J. Zhao, S. Chu and Y. Cui, *Nat Energy*, 2016, DOI:10.1038/NENERGY.2016.10.
- 14 V. Pande and V. Viswanathan, *ACS Energy Lett*, 2019, **4**, 2952–2959.
- 15 S. Cui, P. Zhai, W. Yang, Y. Wei, J. Xiao, L. Deng and Y. Gong, *Small*, 2020, 1905620 DOI:10.1002/sml.201905620.
- 16 W. Chen, R. V. Salvatierra, M. Ren, J. Chen, M. G. Stanford and J. M. Tour, *Advanced Materials*, 2020, 2002850, DOI:10.1002/adma.202002850.
- 17 N. Li, W. Wei, K. Xie, J. Tan, L. Zhang, X. Luo, K. Yuan, Q. Song, H. Li, C. Shen, E. M. Ryan, L. Liu and B. Wei, *Nano Lett*, 2018, **18**, 2067–2073.
- 18 M. Kurniawan and S. Ivanov, *Energies (Basel)*, 2023, **16**, 4933.
- 19 A. A. Assegie, J. H. Cheng, L. M. Kuo, W. N. Su and B. J. Hwang, *Nanoscale*, 2018, **10**, 6125–6138.
- 20 A. A. Assegie, C. C. Chung, M. C. Tsai, W. N. Su, C. W. Chen and B. J. Hwang, *Nanoscale*, 2019, **11**, 2710–2720.
- 21 Z. T. Wondimkun, T. T. Beyene, M. A. Weret, N. A. Sahalie, C. J. Huang, B. Thirumalraj, B. A. Jote, D. Wang, W. N. Su, C. H. Wang, G. Bruncklaus, M. Winter and B. J. Hwang, *J Power Sources*, , DOI:10.1016/j.jpowsour.2019.227589.
- 22 Z. Tu, M. J. Zachman, S. Choudhury, K. A. Khan, Q. Zhao, L. F. Kourkoutis and L. A. Archer, *Chemistry of Materials*, 2018, **30**, 5655–5662.
- 23 R. Weber, M. Genovese, A. J. Louli, S. Hames, C. Martin, I. G. Hill and J. R. Dahn, *Nat Energy*, 2019, **4**, 683–689.
- 24 T. M. Hagos, G. B. Berhe, T. T. Hagos, H. K. Bezabh, L. H. Abrha, T. T. Beyene, C. J. Huang, Y. W. Yang, W. N. Su, H. Dai and B. J. Hwang, *Electrochim Acta*, 2019, **316**, 52–59.
- 25 T. T. Beyene, H. K. Bezabh, M. A. Weret, T. M. Hagos, C.-J. Huang, C.-H. Wang, W.-N. Su, H. Dai and B.-J. Hwang, *J Electrochem Soc*, 2019, **166**, A1501–A1509.
- 26 M. Genovese, A. J. Louli, R. Weber, S. Hames and J. R. Dahn, *J Electrochem Soc*, 2018, **165**, A3321–A3325.
- 27 G. García, S. Dieckhöfer, W. Schuhmann and E. Ventosa, *J Mater Chem A Mater*, 2018, **6**, 4746–4751.
- 28 J. Zhang, Z. Zhou, Y. Wang, Q. Chen, G. Hou and Y. Tang, *ACS Appl Mater Interfaces*, 2022, **14**, 50414–50423.
- 29 H. Yang, E. O. Fey, B. D. Trimm, N. Dimitrov and M. S. Whittingham, *J Power Sources*, 2014, **272**, 900–908.
- 30 Q. Li, S. Tan, L. Li, Y. Lu and Y. He, *Sci. Adv.*, 2017;3:e170124.
- 31 F. M. Wang, H. Y. Wang, M. H. Yu, Y. J. Hsiao and Y. Tsai, *J Power Sources*, 2011, **196**, 10395–10400.
- 32 F. M. Wang, J. C. Wang and J. Rick, *Electrochim Acta*, 2014, **147**, 582–588.
- 33 G. Garcia, E. Ventosa and W. Schuhmann, *Appl. Mater. Interfaces*, 2017, **9**, 18691–18698.

- 34 C. Y. Chen, M. Yoshiba, T. Nagoshi, T. F. M. Chang, D. Yamane, K. Machida, K. Masu and M. Sone, *Electrochem commun*, 2016, **67**, 51–54.
- 35 J. B. Marro, T. Darroudi, C. A. Okoro, Y. S. Obeng and K. C. Richardson, *Thin Solid Films*, 2017, **621**, 91–97.
- 36 K. Cicvarić, L. Meng, D. W. Newbrook, R. Huang, S. Ye, W. Zhang, A. L. Hector, G. Reid, P. N. Bartlett and C. H. K. de Groot, *ACS Omega*, 2020, 5, 14679–14688.
- 37 X. Sun, X. Zhang, Q. Ma, X. Guan, W. Wang and J. Luo, *Angewandte Chemie - International Edition*, 2020, 59, 6665–6674.
- 38 M. Schlesinger and M. Paunovic, *Modern Electroplating*, John Wiley & Sons, Inc., Fourth., 2000.
- 39 Y. Liu, R. Zhang, J. Wang and Y. Wang, 2021, 24, 102332 , DOI:10.1016/j.isci.
- 40 B. Zhang, L. Merker, A. Sanin and H. S. Stein, *Digital Discovery*, 2022,1,755–762.